A thermodynamically consistent poro-visco-elastic model of the Extracellular Matrix

Giulia Laura Celora

Mathematical Institute, University of Oxford

Abstract.

1 Introduction

In tissues, cells are mainly surrounded by extracellular matrix (ECM), a soft porous media mixed with interstitial fluid and made up of networks of polymer chains and charged proteins. *In vitro* studies have shown that ECM rigidity and shear stresses due to the flow of interstitial fluid can promote malignant phenotypes in a population of initially normal cells, impact on cell proliferation and differentiation [8]. Further experiments have shown that tumour development is often associated with a stiffening of the tissue compared to the surrounding healthy one [39]. This causes cells to be exposed to higher compressive stresses and the blood vessels to collapse, thus impeding the diffusion of substances in the extra-cellular environment. Hence, numerous therapies are less effective [45]. Based on such evidence, it is now widely accepted that, unlike originally thought, biological process are not simply regulated by biochemical signals but by the complex interplay of mechanical and chemical stimuli.

Given the different physical nature and scale of phenomena involved, coupling micro-environment and cell behaviours is a problem of high complexity. This requires understanding processes occurring at different temporal and spatial scales and how they interplay to determine the macroscopic behaviour of a tissue, whether healthy or damaged. Despite experiments probing the micro-scale are nowadays possible, these are usually limited to controlled environment in contrast to *in vivo* conditions. On the other hand, we can easily measure macroscopic properties of tissue. Hence, we need quantitative models able to link this tissue to cellular scale, so to extrapolate from the data information the environment cell perceive. In order for this to be possible, alongside experiments, it is necessary to develop a theoretical framework able to capture both the biology and physics involved and which is consistent with the known universal laws of Nature [27]. Having such knowledge on the cell micro-environment can lead to the development of novel therapies and completely change our approach to drug design.

As it will be discussed in Section 2, the ECM can be classified as polyelectrolyte gel [44,45], i.e. hydrogels with charged group. Besides being largely

present in the natural world, synthetic polyelectrolytes are currently employed for a wide range of applications, such as drug delivery, biomedical devices, scaffolds for tissue engineering and soft robotics [7,12,13,32]. Hence, there has been a growing interest in the soft matter community in understanding their behaviour and translating it into mathematical models. In particular, research has been focusing on the phenomena of swelling, i.e. large deformation due to absorption of water, and the diffusion transport and release of solution [15,16,23,46].

With the development of new experimental techniques such as Atomic Force Microscopy (AFM), the local mechanical properties of a material can be measured with nanometre precision [25]. When tested at this scale, soft tissues, as well as hydrogels, have been found to be visco-elastic [31]. As their solid skeleton, i.e. polymer network, is deformed, it can change its conformation to a most entropically favourable one thus dissipating energy. Where purely elastic solids deformed instantaneously, viscoelastic materials instead have time-dependent deformation due to the irreversible nature of the process. Despite these experimental evidences, theoretical studies on visco-elastic soft materials remain limited. Most of the literature has been proposing poro-elastic models, which account for the dissipation of energy due to the transport of solutions but neglect the visco-elastic response of the material itself [9]. While this assumption might be valid for certain applications, the empirical studies previously mentioned highlight the need of including this component in the study of living tissues.

Our works aims to develop a continuum mathematical model of the extracellular matrix which is consistent with the laws of thermodynamics, which accounts for its poro-visco-elastic properties and the coupling of mechanical, transport and electrical phenomena. Nonetheless, our results are more widely applicable to the study of polyelectrolyte gels. At our present knowledge, there is no previous work in the literature capturing all these aspects in a thermodynamic consistent model. In [44,45] Xue et al. develop a nonlinear poroelastic theory for ECM, which couples all three physical phenomena but does not include viscous dissipation. In [19], the authors couple mechano-electrophysiological effects including the viscous dissipation but neglect transport; Caccavo et al. [9] propose a poro-viscoelastic model for neutral hydrogel, thus excluding electrical effects. Following these previous work, we will derive our model in the framework of linear non-equilibrium thermodynamics [27] accounting for multiple phases.

As discussed in [25], there are spatial and time scales which allow to decouple visco-elasticity and poro-elasticity. On one hand, nanoscale rheological testing with AFM give us information on the visco-elastic properties of the sample. For sufficiently small beads, the length scale considered in the experiment is so short that poroelastic relaxation is almost instantaneous and thus negligible. Different 1D rheological model are usually applied to fit experimental measurement: the most common for tissues and hydrogels is the *Standard Linear Solid* model, see Figure 1, to fit the experimental data [9,25]. The poro-elastic behaviour can instead be characterized by standard creep-relaxation test on whole sample. In this case, Darcy's law is usually applied to estimate the hydraulic conductivity and thus characterise the transport of fluid in the material [36,25]. Despite

having a good understanding of the two phenomena independently, there has been little attention to investigating how the two couples. Following a typical approach in the framework of large deformation, we will be using a multiplicative decomposition of the deformation gradient to account for the two phenomena simultaneously.

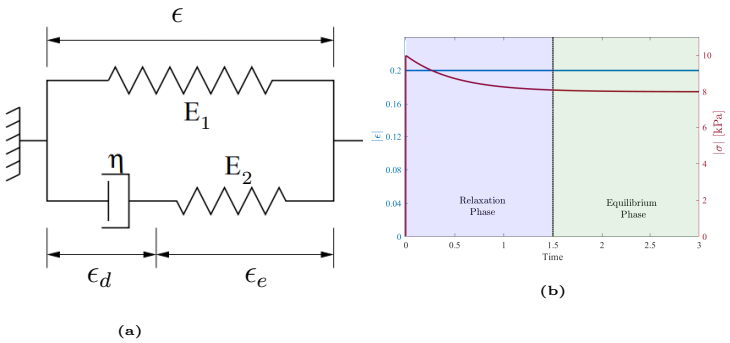

$$\begin{cases} \sigma = E_1\epsilon + E_2\epsilon_d \\ \dot{\epsilon}_e = \dot{\epsilon} - \frac{E_2}{\eta}\epsilon_e = \dot{\epsilon} - \frac{\epsilon_e}{\tau_R} \end{cases} \tag{SLS}$$

Fig. 1: 1D Standard Linear Solid. (a) Rheological Model; (b) Standard Response to a compression test. (1) Differential Equation for the Standard Linear Solid model in the 1D case.

In the framework of large deformation, a standard approach to the study of couple phenomena is the use of a multiplicative decomposition of the deformation gradient. We will be rely on the same idea to build our poro-visco-elatic model. In the literature of soft matter, two possible decomposition have been proposed, based on arbitrary choice, but never systematically compared. As our analysis shows, multiplicative decomposition should be treated as constitutive laws of the material and thus validated and compared. Instead of arbitrarily choosing one of the two, we here develop both approaches, with the aim of identifying their differences and investigating experimental result which would allow us to experimentally test which one best describes the behaviour of soft tissues.

Our work is organized as follows: in Section 2, we discuss more in details the composition of the ECM. We then present a brief overview of Classical Irreversible Thermodynamics, which focuses on the principles later used in the derivation of our model in Section 4. Common [... FOLLOWING SECTIONS TO UPDATE AS I WRITE.]

2 Composition of Extracellular Matrix.

Despite the tissue-specific nature of Extracellular Matrix (ECM), this is usually composed of a network of collagen fibrils entangled with proteoglycans (PGAs) which are covalently bonded to charged chains of glycosaminoglycans (GAGs), see Figure 2a. While collagen is mainly responsible for the mechanical behaviour

of the tissue, GAGs can imbibe water, giving the extracellular matrix the ability to swell while maintaining its structural integrity. As mentioned in the introduction, from this point of view, the ECM is a polyelectrolyte gel. As schematically illustrated in Figure 2(b), polyelectrolyte gels are 3D networks of cross-linked polymer chains that contain ionizable functional groups. When in solution the gel swells, while the functional groups dissociate into fixed charges and mobile ions in the solution. In particular, research has been focusing on the phenomena of swelling, i.e. large deformation due to absorption of water, and the diffusion transport and release of solution [15,16,23,46]. However, only a small fraction of the study published accounts for the visco-elastic properties of the polymer network.

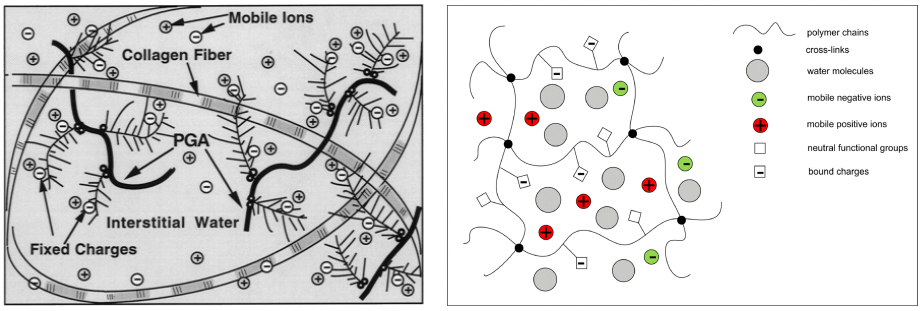

Fig. 2: Analogy between ECM in soft tissue and polyelectrolytes hydrogels: (a) schematic diagram of the structure of the charged hydrated articular cartilage, reproduced from [42]; (b) an anionic polyelectrolyte gel modelled as a three-phase continuum, reproduced from [16].

For the purpose of this study, we will not explicitly distinguish between collagen, PGAs and GAGs. At the tissue level, this can be grouped into a single solid phase (the polymer network), whose mechanical properties are treated as the average over the different components contribution. The interstitial fluid is instead treated as a two-phase solution: the solvent (i.e. water) and the solutes (free ions). The transport of the solution also contributes to the dissipation of energy due to the friction forces generated by the relative motion of the different phases.

As is common in multiphase models of tissue, we will assume that the matrix is isotropic and GAGs are evenly distributed on the network. While this is not a good approximation for tissue like cartilage, which are highly anisotropic, it does apply to the extracellular matrix found in soft tissue such as liver, brain and tumours. It is also important to point out that ECM has additional properties such as thermo-sensitivity and pH-sensitivity. However, both in living organisms and in experimental set-up temperature and pH are maintained fairly constant.

3 Non Equilibrium Thermodynamics.

As mentioned in the introduction, we are interested in studying the deformation of the ECM and the transport of solution in it. Since these are irreversible

processes, they can not be described in the framework of equilibrium thermodynamics.

In the case of irreversible processes, the change in the entropy of a system $\mathrm{d}S$ results from both the reversible exchange of energy and matter with the external environment $\mathrm{d}_e S$ and the internal dissipation of energy during the process $\mathrm{d}_i S$ [27]:

$$\mathrm{d}S = \mathrm{d}_e S + \mathrm{d}_i S, \tag{1}$$

According to the second law of thermodynamics, which applies universally to any system or any of its sub-part $\mathrm{d}_i S \geq 0$. It is important to notice that the second law allows transformations in which total change in entropy dS of the system is negative. This occurs whenever $-\mathrm{d}_e S > \mathrm{d}_i S$ and it can lead to the spontaneous formation of complex and ordered structures such as living organisms. From this point of view, life emerges in physics as an efficient mechanism able to increase sufficiently the entropy of its environment [34].

In this study, we will focus on isothermal processes, i.e. $T = const$, as this well approximate physiological conditions. Under this assumption, as derived by Gurtin in [21], the second law of thermodynamics is equivalent to the following *energy imbalance inequality*:

$$\frac{\mathrm{d}}{\mathrm{d}t}\left\{\int_R \psi\right\} \leq W(R) + M(R) \tag{2}$$

where R is a arbitrary control volume of the system, ψ is the Helmholtz free energy, $W(R)$ is the rate at which the environment does work on R and $M(R)$ is the inflow of mass due to transport. It is important to note that, as long as the quantities involved are well defined, the energy inequality (2) holds for any isothermal process independently of the specific physical system considered. This imposes a constraint on the form of the function ψ and its dependence on the other thermodynamic variables, such as temperature or pressure, which are used to describe the system.

Non-equilibrium thermodynamics mainly focuses on defining the form of $\mathrm{d}_i S$, which, unlike the reversible entropy production $\mathrm{d}_e S$, is not a state variable but depends on the specific transformation applied to the system. Different theories have been proposed, [27], each with its assumptions and specific domain of applicability. In our study we will focus on "Classical Irreversible Thermodynamics" (CIT) which was pioneered by Onsager [38] and Prigogine [40] in the first half of the 20th century. One the most important assumptions of this theory is the *Local Equilibrium Hypothesis*, which guarantees thermodynamic variables, including entropy, are locally well-defined, [27]. Consequently, we can introduce the entropy density $s = s(\mathbf{x}, t)$ such that:

$$S = \int_R s \,\mathrm{d}V, \qquad \mathrm{d}s = \mathrm{d}_e s + \mathrm{d}_i s, \qquad \mathrm{d}_i s > 0, \tag{3}$$

and the local entropy production:

$$\sigma \equiv \frac{\mathrm{d}_i s}{\mathrm{d}t} \geq 0. \tag{4}$$

Another central aspect of the theory is the introduction of *thermodynamic forces* [1] F_m (causes) and *thermodynamic fluxes* J_m (effects) to describe the time evolution of the system during an irreversible transformation. These are related to σ as follows:

$$\sigma = \sum_m F_m J_m \geq 0. \tag{5}$$

While the local equilibrium hypothesis is at the basis of most theories of non-equilibrium thermodynamics, the following two hypotheses uniquely identify CIT:

1. *Linear Relation between forces F and fluxes J*:
$$J_m = \sum_k L_{mk} F_k, \tag{6}$$
where the constant L_{mk} are referred to as **phenomenological coefficients**;
2. *Microscopic Reversibility*: time reversibility of processes at the micro-scale.

Starting from these two principles, in his seminal paper [38] Onsager derives the well-known *Onsager Reciprocal Relation*:

$$L_{mk} = L_{km}. \tag{7}$$

If we now consider an isothermal transformation in the framework of CIT, alongside with the energy imbalance inequality, we have that the following must hold:

$$W(R) + M(R) - \frac{\mathrm{d}}{\mathrm{d}t}\left\{\int_R \psi\right\} = T\int_R \sigma \,\mathrm{d}V\,, \tag{8}$$

In the past few decades, CIT has been applied successfully to the modelling of several physical phenomena of interest for engineers, physicists and applied mathematicians. However, its validity is limited to phenomena near-equilibrium, for which a linear approximation of the flux-force relation holds. The growing interest in more complex far-from-equilibrium phenomena has pushed toward the development of a more general framework for the study of a non-equilibrium phenomena. Since this goes beyond the purpose of our study, we will not discuss it further. We do, however, highlight the law of steepest entropy ascent, which, according to Beretta [3], seems to emerge as the fourth fundamental law of nature. In the linear regime, this principle can be used to prove Onsager's reciprocal relation [2], with no reference to the microscopic reversibility hypothesis, whose validity remains instead controversial [30].

4 Model Development

4.1 Conservation Law.

As mentioned in Section 2, we here consider the ECM as a three-phase medium composed of a solid polymer network with fixed charges, a solvent (i.e. water molecules, interstitial fluid) and solutes (freely moving charges).

[1] Not to be intended in the mechanical sense

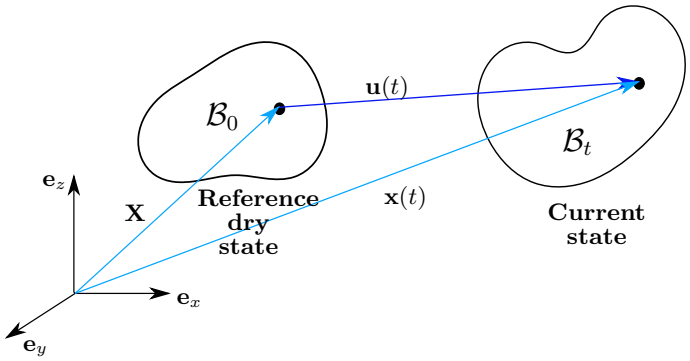

Fig. 3: Sketch of the dry and current state of the ECM network.

As the tissue deforms, the material element originally located at $\mathbf{X}$ in the initial configuration $\mathcal{B}_0$ is displaced to the point $\mathbf{x}$ in the current configuration $\mathcal{B}_t$, see Figure 3. Such transformation is described by the deformation gradient tensor $\mathbb{F} = \partial\mathbf{x}/\partial\mathbf{X}$; the information about the change in ECM volume is encoded in $J = \det\mathbb{F}$. As in [22], we consider the reference, or initial, state $\mathcal{B}_0$, which is stress free, to be equivalent to the dry stage of the ECM, i.e. only solid phase present. Since we assume the solid phase to be incompressible, any change in the volume can only be related to the migration of solvent and solutes molecules, whose nominal [2] concentrations will be denoted by C_s and C_i respectively, $i = 1, \ldots, N$ with N being the number of free ion species. This lead to the molecular incompressibility condition:

$$J = 1 + v_s C_s + \sum_{i=1}^{N} v_i C_i \tag{9}$$

where v_m are the characteristic molecular volume of each species in the solution. When considering the interstitial fluid, the contribution of ions to the volume can be neglected [44,45] so that Equation (9) reduces to:

$$J = 1 + v_s C_s. \tag{10}$$

Consequently, the volume fractions of fluid ϕ_f and solid ϕ_n phases in the swollen ECM are defined as:

$$\phi_f = \frac{v_s C_s}{1 + v_s C_s}, \qquad \phi_n = \frac{1}{1 + v_s C_s}. \tag{11}$$

where again we are neglecting the contribution of ions to the total volume. While C_m denote the number of each molecule per unit volume in the initial configuration for the m-th species in the solution, the actual concentration in the current state is denoted by $c_m = C_m/J$. Throughout the derivation of the model, we will be using the index $i = 1, \ldots, N$ to denote the ionic species only,

[2] variable value in the reference configuration.

while $m \in \{s, 1, \dots, N\}$ refers to all mobile species, i.e. both the solvent and solutes.

Mass conservation must apply to all mobile species and in the initial configuration this reads:

$$\dot{C}_m + \nabla_0 \cdot \mathbf{J}_m = 0, \tag{12}$$

where $\mathbf{J}_m$ is the nominal flux per unit area in the dry state, $\dot{C}_m$ is the derivative of C_m with respect to time, i.e. $\dot{C}_m \equiv \partial_t C_m$ and ∇_0 denote the gradient in the Lagrangian coordinates $\mathbf{X}$. Their counterparts in the actual configuration are denoted by $\mathbf{j}_m$ and ∇ and are defined according to the following rules:

$$\mathbf{J}_m = J\mathbb{F}^{-1}\mathbf{j}_m, \qquad \nabla_0(\cdot) = \mathbb{F}^T\nabla(\cdot). \tag{13}$$

When considering tissues or hydrogels, inertial and gravitational effect are commonly neglected, so that the conservation of momentum for the ECM reads:

$$\nabla_0 \cdot \mathbb{S} = 0, \tag{14}$$

where $\mathbb{S}$ is the first Piola-Kirchoff tensor, which represents the stress state of the ECM in the initial configuration. The counterpart in the current configuration is the Cauchy stress tensor $\mathbb{T}$, which is related to $\mathbb{S}$ as follows:

$$\mathbb{T} = J^{-1}\mathbb{S}\mathbb{F}^T. \tag{15}$$

The presence of free moving ions generates an electric field which is denoted by $\mathbf{E}$ and $\mathbf{e}$ in the initial and current configuration respectively. Introducing the electrostatic potential Φ, we have that:

$$\mathbf{E} = -\nabla_0 \Phi, \qquad \mathbf{e} = -\nabla \Phi. \tag{16}$$

As in [23], we consider the matrix to be a dielectric material[3]. Consequently, the presence of the electric field generates an electric displacement $\mathbf{H}$[4], which must obey Gauss law of electrostatics:

$$\nabla_0 \cdot \mathbf{H} = Q, \tag{17}$$

where Q is the local total charge, which accounts for both fixed and moving charges:

$$Q = e\left(\sum_i z_i C_i + z_f C_f\right), \tag{18}$$

where e is the elementary charge, C_f is the concentration of fix charges and z_m is the valence of the corresponding charged species. Note that C_f here corresponds

[3] a material that does not conduct electricity but can be polarized in the presence of an electric field.

[4] the vector field that accounts for both the electric field and the polarization of the dielectric material.

to the concentration of GAGs, which is assumed to be a constant a fraction of C_s. As for above, we can move from nominal quantities to the corresponding value in the current configuration by applying the following rules:

$$\mathbf{H} = J\mathbf{h}\mathbb{F}^{-T}, \tag{19}$$

$$\mathbf{E} = \mathbb{F}^{T}\mathbf{e}, \tag{20}$$

where $\mathbf{h}$ is the electric displacement in the current configuration.

4.2 Kinematics.

As mentioned in the introduction, we model the ECM as a poro-visco-elastic material, with particular interest in the viscous aspect of the material. As shown in Figure 4, there are two molecular processes that give rise to the macroscopic time-dependent response of the system:

1. the rearrangements of molecules at the micro-scale, which has entropic origin and result in a volume-preserving viscous deformation;
2. the long range transport of fluid that leads to swelling, i.e. changes in the ECM's size, and give rise to frictional forces between phases.

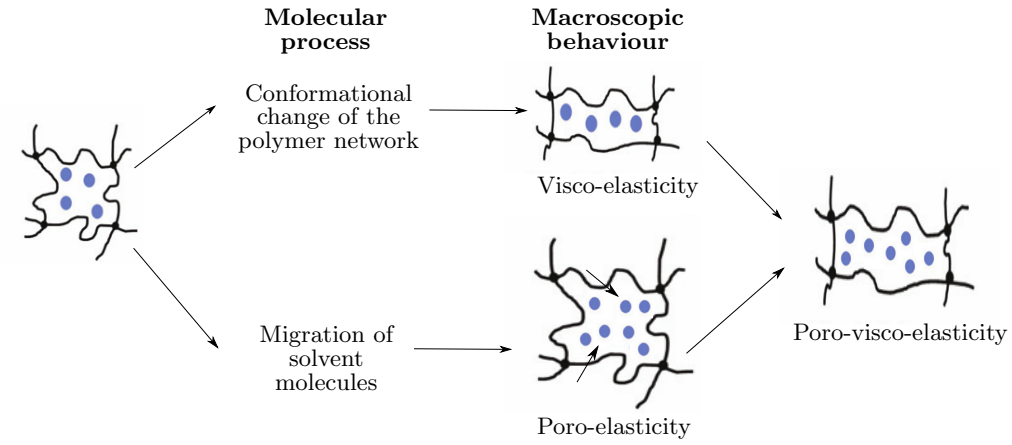

Fig. 4: Illustration of the molecular processes which account for the macroscopic deformation of ECM: viscosity is related to change in the conformation of the network which preserve the volume of the network.

As illustrated in Figure 4, at the microscopic level this results in a visco-elastic and poro-elastic behaviour respectively.

In order to capture both phenomena, as common in the large-deformation theory [9,10,1,20,37,43] and first proposed by Kröner in 1960 [28], we consider a multiplicative decomposition of the deformation tensor $\mathbb{F}$. As this can be choose

arbitrary, different decomposition have been proposed in the literature. We will here consider the two most commonly used, which will be here denoted as model A [9,10,1] and model B [20,37,19]:

$$\text{MODEL A} \Rightarrow \begin{cases} \mathbb{F} = \mathbb{F}_e \mathbb{F}_v, \\ \det \mathbb{F}_v = 1, \quad \det \mathbb{F}_e = \det \mathbb{F} \end{cases} \tag{A}$$

$$\text{MODEL B} \Rightarrow \begin{cases} \mathbb{F} = \mathbb{F}_{vol} \bar{\mathbb{F}} = \mathbb{F}_{vol} \bar{\mathbb{F}}_e \bar{\mathbb{F}}_v \\ \det \mathbb{F} = \det \mathbb{F}_{vol}, \quad \det \bar{\mathbb{F}} = \det \bar{\mathbb{F}}_e = \det \bar{\mathbb{F}}_v = 1. \end{cases} \tag{B}$$

Comparing the two, we note that the only difference is that in model B the volumetric deformation, $\mathbb{F}_{vol}$, is decoupled from the deviatoric one, $\bar{\mathbb{F}}$. To the best of our knowledge, there is no previous systematic study in the literature that compares these two approaches. While the two model are identical in the case of iso-volumetric deformation, i.e. $\det \mathbb{F} = J = 1$, this is not always the case when a tissue swells. As it will be clear in Section 6, the choice of how to decompose the vector $\mathbb{F}$ can not be arbitrary but should instead be treated as a constitutive assumption on the material properties. This highlights the need of experimental testing to validate which model better describe the material studied.

As an explanatory example on how mathematical models can be derived in the non-equilibrium thermodynamics framework, we will fully here derive the governing equation for model A. The interested reader can find the details of the derivation for model B in Appendix D.

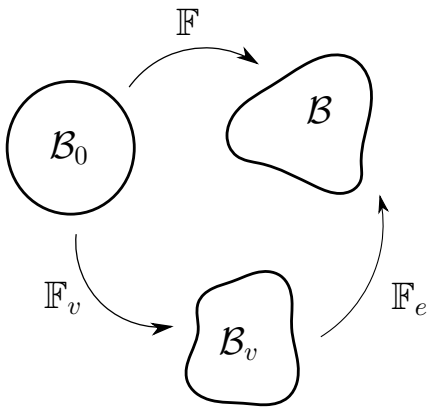

Fig. 5: multiplicative decomposition corresponding to model A, Equation (A).

Looking back at System (A), we identify $\mathbb{F}_e$ as the elastic contribution to the deformation while, the term $\mathbb{F}_v$ accounts for the viscous flow. As illustrate in Figure 5, the multiplicative decomposition is equivalent to introducing an intermediate configuration $\mathcal{B}_v$, called the natural or virtual configuration. The evolution of the natural configuration can be interpreted as an entropy produc-

ing, i.e. dissipative, process. On the other hand, in the elastic deformation from the natural to the current configuration all the energy is stored in the system.

Using Equation (A), we can compute the velocity gradient tensor $\mathbb{L}$:

$$\mathbb{L} = \dot{\mathbb{F}}\mathbb{F}^{-1} = \mathbb{L}_e + \mathbb{F}_e\mathbb{L}_v\mathbb{F}_e^{-1}, \tag{21}$$

where $\mathbb{L}_e = \dot{\mathbb{F}}_e\mathbb{F}_e^{-1}$ and $\mathbb{L}_v = \dot{\mathbb{F}}_v\mathbb{F}_v^{-1}$ are respectively the elastic and viscous velocity gradient tensor. These can be decomposed in their symmetric $\mathbb{D}$ and skewed $\mathbb{W}$ part:

$$\begin{aligned} \mathbb{L}_e = \mathbb{D}_e + \mathbb{W}_e, \quad \mathbb{D}_e = \frac{\mathbb{L}_e + \mathbb{L}_e^T}{2}, \quad \mathbb{W}_e = \frac{\mathbb{L}_e - \mathbb{L}_e^T}{2}; \\ \mathbb{L}_v = \mathbb{D}_v + \mathbb{W}_v, \quad \mathbb{D}_v = \frac{\mathbb{L}_v + \mathbb{L}_v^T}{2}, \quad \mathbb{W}_v = \frac{\mathbb{L}_v - \mathbb{L}_v^T}{2}. \end{aligned} \tag{22}$$

The decomposition (A) is not unique, as stress state in $\mathcal{B}_v$ would not change under any arbitrary rigid-body rotation [33]. As suggested by [1], in the case of isotropic material, it is reasonable to assume the viscous flow to be irrotational, i.e. $\mathbb{W}_v = \mathbb{O}$, so that $\mathbb{L}_v \equiv \mathbb{D}_v$. As mentioned before, the physical nature of the viscous deformation is molecular rearrangement so that volume is preserved. This requires to introduce the additional constraint:

$$J_v = \det \mathbb{F}_v = 1. \tag{23}$$

4.3 Energy Balance Inequality.

As mentioned in Section 3, in a thermodynamically consistent model, the free energy ψ can not be chosen arbitrarily but needs to satisfy the energy imbalance inequality, (2). In this section, we focus on the right-hand side of the inequality which specify how the system exchanges energy and mass with the environment. Considering a control volume R in the reference configuration $\mathcal{B}_0$, the system exchanges mass due to the diffusion of each mobile species, so that $M(R)$ is given by:

$$M(R) = \sum_{m=s,1,\dots,N} -\int_{\partial R} \mu_m \, \mathbf{J}_m \cdot \mathbf{n} \tag{24}$$

where $\mathbf{n}$ is the unit normal vector to the surface ∂R and μ_m is the chemical potential associated with each species. Widely used in the thermodynamics of mixture, the chemical potential is a measure of the rate of change in free energy associated with adding one more molecule to a unit volume.

The term $W(R)$, i.e. the rate of work done on the system, is instead decomposed in two contributions, the rate of electrical $W_{el}(R)$ and mechanical work $W_{mec}(R)$. Following [16], $W_{el}(R)$ is defined as:

$$W_{el}(R) = -\int_{\partial R} \Phi \, \dot{\mathbf{H}} \cdot \mathbf{n} \tag{25}$$

while $W_{mec}(R)$ reads:

$$W_{mec}(R) = \int_{\partial R} \mathbb{S}\mathbf{n} \cdot \dot{\mathbf{u}} \tag{26}$$

where $\mathbf{u} = \mathbf{x} - \mathbf{X}$ is the displacement vector, which is related to the deformation tensor by $\mathbb{F} = \mathbb{I} - \nabla_0 \mathbf{u}$. Substituting this result back into the formula (2) and applying the divergence theorem we obtain the following inequality:

$$\int_R \dot{\psi} - \mathbf{E} \cdot \dot{\mathbf{H}} + \sum_{i=1}^{N} \left[e\Phi z_i \dot{C}_i + \nabla_0 \left(\mu_i \mathbf{J}_i \right) \right] + \nabla_0 (\mu_s \mathbf{J}_s - \mathbb{S}^T \dot{\mathbf{u}}) \leq 0 \tag{27}$$

Since this must hold for any choice of the volume R, the inequality must hold also locally:

$$\dot{\psi} - \mathbf{E} \cdot \dot{\mathbf{H}} + \sum_{i=1}^{N} \left[e\Phi z_i \dot{C}_i + \nabla_0 \left(\mu_i \mathbf{J}_i \right) \right] + \nabla_0 (\mu_s \mathbf{J}_s - \mathbb{S}^T \dot{\mathbf{u}}) \leq 0. \tag{28}$$

Further accounting for Equations (12)-(14), we obtain that:

$$\dot{\psi} - \mathbf{E} \cdot \dot{\mathbf{H}} + \sum_{i=1}^{N} \left[e\Phi z_i - \mu_i \right] \dot{C}_i - \mu_s \, \dot{C}_s - \mathbb{S} : \dot{\mathbb{F}} + \sum_m \nabla_0 \, \mu_m \cdot \mathbf{J}_m \leq 0. \tag{29}$$

As exhaustively discussed in previous studies [1,21], the energy inequality imposes restrictions on the constitutive equation of the free energy ψ. Adapting their results to our specific problem, we have that:

$$\psi = \psi(\mathbb{F}, \mathbb{F}_e, C_s, C_i, \mathbf{H}), \tag{30}$$

which precludes any explicit dependency of ψ on the chemical potential or the viscous deformation gradient $\mathbb{F}_v$. By differentiating the incompressibility condition (10) and (23), we obtain:

$$v_s \dot{C}_s - J\mathbb{F}^{-T} : \dot{\mathbb{F}} = 0, \tag{31}$$

$$\mathbb{I} : \mathbb{L}_v = 0. \tag{32}$$

If we now substitute (30) into (29), and include the constraint (31)-(32) using as Lagrange multipliers p and p_v respectively, we are left with the augmented form of the energy imbalance inequality:

$$\begin{aligned} \left(\frac{\partial \psi}{\partial C_s} - \mu_s + pv \right) \dot{C}_s + \left(\frac{\partial \psi}{\partial \mathbf{H}} - \mathbf{E} \right) \cdot \dot{\mathbf{H}} + \sum_i \left(\frac{\partial \psi}{\partial C_i} + e\Phi z_i - \mu_i \right) \dot{C}_i \\ + \left(\frac{\partial \psi}{\partial \mathbb{F}} + \frac{\partial \psi}{\partial \mathbb{F}_e} \mathbb{F}_v^{-1} - \mathbb{S} - pJ\mathbb{F}^{-T} \right) : \dot{\mathbb{F}} + \sum_m \nabla_0 \, \mu_m \cdot \mathbf{J}_m \\ - \left(\mathbb{F}_e^T \frac{\partial \psi}{\partial \mathbb{F}_e} - p_v \mathbb{I} \right) : \mathbb{L}_v \leq 0. \end{aligned} \tag{33}$$

Note that in deriving (33), we have also made us of the following identity:

$$\dot{\mathbb{F}} = \dot{\mathbb{F}}_e \mathbb{F}_v + \mathbb{F}_e \dot{\mathbb{F}}_v \Longrightarrow \dot{\mathbb{F}}_e = \dot{\mathbb{F}} \mathbb{F}_v^{-1} - \mathbb{F}_e \mathbb{L}_v. \tag{34}$$

4.4 Construction of the Free Energy.

Having the general form of ψ, Equation (30), it remains to construct its precise form. Following a standard approach in ψ-depending modeling, we assume that the total free energy can be additively decomposed with each physical mechanisms contributing independently. We here consider five distinct contributions:

- the energy of the electric field ψ_1;
- the energy of solvent and solutes' molecules not interacting with the solid phase ψ_2;
- the energy of mixing the solid phase with the solution, ψ_3;
- the energy of mixing the solvent with the solutes in solution, ψ_4;
- the energy of the solid phase not interacting with the solution, ψ_5.

Assuming the solid phase to be an ideal and linear dielectric material, with constant permittivity ϵ, the free energy of polarization reads [15,23]:

$$\psi_1 = \frac{1}{2\epsilon J}\mathbf{H}\mathbb{F}^T \cdot \mathbb{F}\mathbf{H}. \tag{35}$$

The specific energy density ψ_2 has the standard form:

$$\psi_2 = \sum_m \mu_m^0 C_m \tag{36}$$

where μ_m^0 denotes the chemical potential of non interacting solvent and ions molecules. According to Flory-Huggins theory [17,26] of mixtures, the mixing energy is given by:

$$\psi_3 = \frac{k_B T J}{v_s}\left(\phi_f \ln \phi_f + \chi \phi_f \phi_n\right), \tag{37}$$

where k_B is the Boltzmann's constant, T is the temperature and χ is the Flory-Huggins parameter, which is a measure of the enthalpy of mixing. Note that Xue et al.[44,45] use a different approach. In these studies, the authors assume only the mixing of GAGs with solvent, while neglecting the collagen. Since we are considering GAGs and the collagen network as as a unique solid phase and we could not find any evidence that collagen does not mix with water, we have chosen the more general form (37).

As the interstitial fluid is well approximated by a dilute solution, the contribution ψ_4 reads [23,44,45]:

$$\psi_4 = k_B T \sum_{i=1}^{N} C_i \left(\ln \frac{C_i}{C_s} - 1\right). \tag{38}$$

Finally, we need to specify the strain energy ψ_5 which depends on the particular constitutive model used to describe the material. As mentioned in the Introduction the Standard Linear Solid (SLS), see Figure 1, is commonly used to describe soft material in the regime of small deformation. However, when account for large deformation, as in the case of swelling, soft material present a

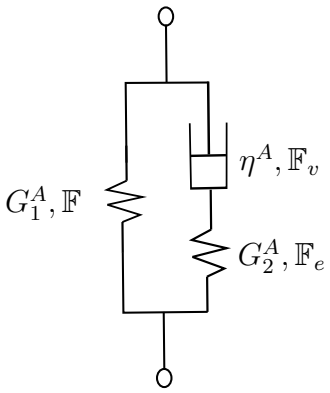

(a)

Element	Constitutive Properties	Deformation
spring 1	Isotropic Neo-Hookean spring	volumetric + deviatoric
spring 2	Isotropic Neo-Hookean spring	volumetric + deviatoric
dashpot	Isotropic Linear dashpot	deviatoric

(b)

Fig. 6: (a) Schematic representation of the non-linear rheological model for ECM; (b) Table summarizing the major properties of the model components.

non-linear behaviour [18]. For this reason we consider the model in Figure 6a, which is a generalization of the 1D SLS to 3D problems with non-linear elastic response.

The strain energy can thus be decomposed into the sum of the contributions from spring 1 and spring 2:

$$\psi_6 = \psi_{5.1}(\mathbb{F}) + \psi_{5.2}(\mathbb{F}_e). \tag{39}$$

As in [45], we consider the spring to be isotropic and hyper-elastic (Neo-Hookean) which are characterised by the following form of the free-energy:

$$\psi_{5.1}(\mathbb{F}) = \frac{G_1^A}{2}\left(\mathbb{F} : \mathbb{F} - 3 - 2\ln J\right) \tag{40}$$

$$\psi_{5.2}(\mathbb{F}_e) = \frac{G_2^A}{2}\left(\mathbb{F}_e : \mathbb{F}_e - 3 - 2\ln J_e\right) \tag{41}$$

where $G_{1/2}$ stands for the shear modulus associated with each spring, $J_e = \det \mathbb{F}_e$, while J is as defined in the previous sections. As derived in [18], the hyper-elastic model (41) can be correlated to the microscopic properties of a polymer network, under the assumption of Gaussian chains and affine deformation. Other thermodynamically consistent form of the stretching energy have been proposed in the literature [4,6,14]. These have been also derived by statistical arguments but starting from different network models.

4.5 Entropy Production $\boldsymbol{\sigma}$.

Having specified how the system interacts with its environment, we can now discuss how it dissipates energy. As mentioned in Section (4.2), there are two contributions: transport (diffusion of solvent and solutes) and viscosity. The

thermodynamic fluxes [5] associated with these two phenomena are $\mathbf{J}_m$, $m = s, 1, \ldots, N$, and $\mathbb{L}_v$. Consequently, using Equation (5), we obtain:

$$\sigma = \sum_m \zeta_m \cdot \mathbf{J}_m + \zeta_v : \mathbb{L}_v, \tag{42}$$

where ζs represent the thermodynamic forces associate with each flux. On the other hand, $\dot{C}_s$, $\dot{C}_i$, $\dot{\mathbf{H}}$ and $\dot{\mathbb{F}}$ describe the evolution of reversible process. This implies that their value can be controlled and arbitrarily chosen, by carefully tune the condition of an experiment, i.e. tuning boundary and initial conditions. In order for the energy imbalance inequality (33) to always hold, and given the constraint (30) on ψ, this can only happen if the terms highlighted in blue in Equation (33) are identically zero. As shown in the Appendix B, this leads to the following system of state equations:

$$\begin{aligned}\mu_s = pv_s + \mu_s^0 + k_B T \Bigg[&\ln \frac{C_s v_s}{1 + C_s v_s} + \frac{1}{1 + C_s v_s} \\ &+ \frac{\chi}{(1 + C_s v_s)^2} - \sum_i \frac{C_i}{C_s} \Bigg],\end{aligned} \tag{43}$$

$$\mu_i = \mu_i^0 + e\Phi z_i + kT \ln \frac{C_i}{C_s}, \tag{44}$$

$$\mathbf{E} = \frac{1}{\epsilon J} \mathbb{F}^T \mathbb{F}\, \mathbf{H}\,, \qquad -\epsilon J \nabla^2 \Phi = Q\,, \tag{45}$$

$$\begin{aligned}\mathbb{T} = -p\mathbb{I} + \frac{G_1^A}{1 + C_s v_s} (\mathbb{B} - \mathbb{I}) + \frac{G_2^A}{1 + C_s v_s} (\mathbb{B}_e - \mathbb{I}) \\ + \underbrace{\epsilon \left[\frac{1}{2} |\nabla \Phi|^2 \mathbb{I} - \nabla \Phi \otimes \nabla \Phi \right]}_{\mathbb{T}^{Max}},\end{aligned} \tag{46}$$

where T^{max} is the component of the stress tensor due to the presence of the electric field. As discussed in Section 3, in the framework of linear non-equilibrium thermodynamics, when considering isothermal transformation, the second law of thermodynamics can be rewrite as Equations (8). Using the same argument as in Section 4.3 and Equation (42), we can rewrite Equations (8) in differential form, and substituting Equations (43)-(46), we obtain:

$$\sigma = -\sum_m \frac{1}{T} \nabla_0 \mu_m \cdot \mathbf{J}_m + \frac{1}{T} \left(\mathbb{F}_e^T \frac{\partial \psi}{\partial \mathbb{F}_e} - p_v \mathbb{I} \right) : \mathbb{L}_v \tag{47}$$

[5] See Section 3

Equating Equation (47) and (42), it is evident that the thermodynamics forces are:

$$\zeta_m = \frac{1}{T}\nabla_0 \mu_m, \tag{48}$$

$$\zeta_v = \frac{1}{T}\left(\mathbb{F}_e^T \frac{\partial \psi}{\partial \mathbb{F}_e} - p_v \mathbb{I}\right) = \frac{1}{T}\left[G_2^A(\mathbb{C}_e - \mathbb{I}) - p_v \mathbb{I}\right]. \tag{49}$$

Assuming to be in regime of linear non-equilibrium thermodynamics, we can use the identity (6) to couple fluxes and forces. However, considering the symmetry constraint from *Curie's law*[6] , there can be no coupling between fluxes and forces of different tensorial nature. Consequently, we are left with the following force-flux relation:

$$\mathbb{L}_v = L_{vv}\zeta_v, \tag{50}$$

$$\mathbf{J}_m = \sum_{k=s,1,..,N} L_{mk}\zeta_k. \tag{51}$$

As described in Appendix C, starting from Equations (48)-(51) and with common consideration from the theory of mixture, we can derive the following system of time dependent equations:

$$\partial_t C_s = \nabla_0 \cdot \left[K C_s \mathbb{F}^{-1}\left(c_s \nabla \mu_s + \sum_i \frac{D_i}{D_i^0} c_i \nabla \mu_i\right)\right], \tag{52}$$

$$\partial_t C_i = \nabla_0 \cdot \left[\frac{D_i}{k_B T} C_i \mathbb{F}^{-1} \nabla \mu_i - \frac{D_i}{D_i^0}\frac{C_i}{C_s}\mathbf{J}_s\right], \tag{53}$$

$$\dot{\mathbb{B}}_e = \mathbb{L}\mathbb{B}_e + \mathbb{B}_e\mathbb{L}^T - \frac{1}{\tau_R}\mathbb{B}_e \mathrm{DEV}[\mathbb{B}_e]. \tag{54}$$

where the parameters (see the Glossary) are macroscopic phenomenological coefficients, that can either be estimated experimentally or derived from the nano/microscopic properties of the different phases [44,45]. To sum up the governing equations for the Model A are Equations (43)-(46) together with the flow rules (52)-(54). The analogous system of equation for model B can be found in Appendix D.

4.6 Evolution Equation.

In order to get a better physical insight into the behaviour, we first rewrite the solvent chemical potential as:

$$\mu_s = \mu_s^0 + k_B T\left(\frac{p v_s}{k_B T} + \Pi_{osm} - \sum_i \frac{C_i}{C_s} - \frac{\gamma J}{k_B T}\Pi_{grad}\right), \tag{55}$$

$$\Pi_{osm} = \ln\frac{C_s v_s}{1 + C_s v_s} + \frac{1}{1 + C_s v_s} + \frac{\chi}{(1 + C_s v_s)^2}, \tag{56}$$

$$\Pi_{grad} = \nabla^2 C_s, \tag{57}$$

[6] Macroscopic causes can not have more element of symmetries than the effect they cause [30]

where p represents the pore pressure, Π_{osm} is the osmotic pressure of the solution and Π_{grad} is the pressure due to interface energy. If we now substitute into Equations (52) the chemical potentials (55)-(44), which yields to:

$$\partial_t C_s = \nabla_0 \cdot \left\{ K\mathbb{F}^{-1} \left[C_s v_s \nabla p - \gamma C_s J \nabla \Pi_{grad} + \sum_i \frac{D_i}{D_i^0} C_i e z_i \nabla \Phi \right.\right. \\ \left.\left. + k_B T \left(C_s \nabla \Pi_{osm} + \sum_i \left(1 - \frac{D_i C_i}{D_i^0 C_s} \right) \nabla C_s - \sum_i \left(1 - \frac{D_i}{D_i^0} \right) \nabla C_i \right) \right] \right\}. \tag{58}$$

The above equation shows that the solvent transport is driven by pressure gradient, osmotic pressure gradient (green term in Equation (58)), electric potential gradient and the additional composition gradient (red term in Equation (58)), which is here first introduced in the context of polyelectrolytes. In the absence of solutes ($C_i \equiv 0$), we recover the same model presented by Hennessy et. al [22]. If we further assume that $|\nabla \Pi_{grad}| << 1$ and take the limit $v_s C_S \to \infty$, Equations (58) reduces to Darcy's law for the flow in a porous media. The model for polyelectrolytes proposed by Hong [23] correspond instead to the limit $D_i^0 \to \infty$, i.e. mobile species can move freely in pure solution, and $|\nabla \Pi_{grad}| << 1$.

Similarly we can rewrite Equation (53) as:

$$\partial_t C_i = \nabla_0 \left[D_i \mathbb{F}^{-1} \left(\underbrace{\nabla C_i}_{\text{diffusion}} + \underbrace{\frac{e C_i z_i}{k_B T} \nabla \Phi}_{\text{electric}} \right) - \underbrace{\frac{D_i C_i}{C_s} \mathbb{F}^{-1} \nabla C_s}_{\text{osmotic pressure}} - \underbrace{\frac{D_i C_i}{D_i^0 C_s} \mathbf{J}_s}_{\text{advenction}} \right] \tag{59}$$

In the case of ions, the driving forces of transport are the diffusion of ions, the electric field, the osmotic pressure due to the mixing with the solvent and the advection term (due to the relative movement of ions with respect to the solvent). In the limit $D_i^0 \to 0$, where the ions can freely move in the pure solution, we recover the formulation of Hong in [23], which is commonly used in the description of polyelectrolytes. In the dilute limit, i.e. when the concentration of ions is much smaller than the solvent concentration $C_i << C_s$, we can drop both the osmotic and advection term so to recover the well-known Nernst-Planck equation [23, see Equation (6.67)].

As mentioned in the introduction, one the major aspect of interest is the visco-elastic contribution to the evolution of the system. Even though in the transport Equation (58)-(59) there is no direct reference to it, the transport is indirectly coupled to the visco-relaxation through the pressure gradient. Taking the divergence of Equation (46) and using the conservation of momentum (14), we can identify components to the pressure gradient:

$$\nabla p = \nabla \cdot \mathbb{T}^{kort} + \nabla \cdot \mathbb{T}^{Max} + G_1^A \underbrace{\nabla \cdot \left[\frac{\mathbb{B} - \mathbb{I}}{1 + v_s C_s} \right]}_{\substack{\text{swelling} \\ \text{+ deviatoric} \\ \text{deformation}}} + G_2^A \underbrace{\nabla \cdot \left[\frac{\mathbb{B}_e - \mathbb{I}}{1 + v_s C_s} \right]}_{\substack{\text{swelling} \\ \text{+ deviatoric} \\ \text{deformation} \\ \text{+ viscous relaxation}}} \tag{60}$$

Differently from the standard Neo-Hookean model for polyelectrolytes, we have an additional term highlighted in red, which accounts for the energy stored in the second spring of model A. Its time evolution, as determined by Equation (54) is driven by the swelling and macroscopic deformation and a relaxation term which capture the viscous nature of the solid phase:

$$\dot{\mathbb{B}}_e = \underbrace{\mathbb{L}\mathbb{B}_e + \mathbb{B}_e\mathbb{L}^T}_{\substack{\text{swelling} \\ \text{+ deviatoric} \\ \text{deformation}}} - \underbrace{\frac{1}{\tau_R}\,\mathbb{B}_e \text{DEV}[\mathbb{B}_e]}_{\substack{\text{viscous} \\ \text{relaxation}}} \tag{61}$$

Despite the introduction of the non-linear terms, there is an apparent analogy between the above Equation and the ODE describing the standard linear solid, see Equation (SLS) in the Introduction. The term $\dot{\epsilon} \leftrightarrow \mathbb{L}$ is related to the strain experienced by spring 1, while $\epsilon_e \leftrightarrow \mathbb{B}_e$ is the variable describing the strain on the 2. In the limit $\tau_R \to \infty$, we have that $\mathbb{B}_e \equiv \mathbb{B}$. We thus recover the standard Neo-Hookean hyper-elastic model for hydrogels with shear modulus given by $G_1^A + G_2^A$. Similar result are obtained for model B. The governing equation of Model B is equivalent to (61), except for the fact that it is not influence by purely volumetric deformation:

$$\dot{\bar{\mathbb{B}}}_e = \underbrace{\bar{\mathbb{L}}\bar{\mathbb{B}}_e + \bar{\mathbb{B}}_e\bar{\mathbb{L}}^T}_{\substack{\text{deviatoric} \\ \text{deformation}}} - \underbrace{\frac{1}{\tau_R}\,\bar{\mathbb{B}}_e \text{DEV}[\bar{\mathbb{B}}_e]}_{\substack{\text{viscous} \\ \text{relaxation}}} \tag{62}$$

while the pressure gradient is defined as:

$$\begin{aligned} \nabla p = \nabla \cdot \mathbb{T}^{kort} + \nabla \cdot \mathbb{T}^{Max} + G_1^B \underbrace{\nabla \cdot \left[\frac{\text{DEV}[\bar{\mathbb{B}}]}{1 + v_s C_s}\right]}_{\substack{\text{+ deviatoric} \\ \text{deformation}}} \\ + G_2^B \underbrace{\nabla \cdot \left[\frac{\text{DEV}[\bar{\mathbb{B}}_e]}{1 + v_s C_s}\right]}_{\substack{\text{deviatoric} \\ \text{deformation} \\ \text{+ viscous relaxation}}} + G_{vol} \underbrace{\nabla \left(\frac{J^{2/3} - 1}{J}\right)}_{swelling}. \end{aligned} \tag{63}$$

As we will discuss in the next section, when considering instead a purely volumetric deformation, such as for free swelling, i.e. $\mathbb{F} = \mathbb{F}_{vol} = J^{1/3}\mathbb{I}$, we have that the two model are equivalent given that $G_{vol} \equiv G_A + G_B$. Before comparing the model in different experimental setting, we have briefly summarised in Table (1) the variables and governing equation for both models. In order to have a close solution, the proper boundary and initial conditions needs also to be assigned depending on the specific problem considered.

Variable	Model A	Model B
Solvent Concentration	C_s (58)	
Chemical Potential of the solvent	μ_s (43)	
Ionic Concentrations	C_i (59)	
Chemical Potential of the ions	μ_i (44)	
Local Volumetric Change	J (10)	
Cauchy Stress Tensor	$\mathbb{T}$ (14)	
Deformation Gradient	$\mathbb{F}$ (A)	$\mathbb{F}$ (B)
Pore Pressure	p (46)	p 117)
Left-Cauchy Tensor for spring 2	$\mathbb{B}_e$ (54)	$\bar{\mathbb{B}}_e$ (120)
Viscous Velocity Gradient Tensor	$\mathbb{L}_v$ (89)	$\bar{\mathbb{L}}_v$ (112)
Electric Field	Φ (45)	

Table 1: List of Variables involved in the problem, with reference to the corresponding governing equations.

5 Elasticity: Equilibrium Behaviour.

In this section, we will be focusing on the equilibrium behaviour of the two model under free and compressed swelling. Given the large number of parameter in the models, such experiment allows to estimate a subset of them. While previous model proposed in the literature have been arbitrarily chosen how to decompose the deformation gradient $\mathbb{F}$, we here shows that such choice need to consider equal to a constitutive equation and thus tested experimentally.

5.1 Unconstrained Free Swelling.

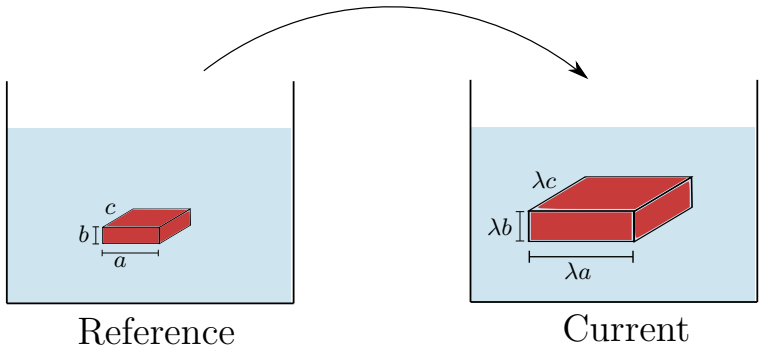

Fig. 7: Schematic representation of a free swelling. Since we are considering an isotropic mixture, the ECM maintains its shape while all dimension are stretched of the same amount λ. So that the relative volume change is $\delta V = \lambda^3 - 1$.

Having derived the set of equations for both model A and model B, we now want to compare how the two behave in different settings. We first look at unconstrained free swelling of a cuboid slice of ECM immersed in a bath of interstitial fluid. For simplicity we consider that contains only two species of free ions, which carry a positive C_+ and a negative C_- charge respectively. We assume the bath to be well-mixed and stress-free with both pressure and electric potential identically zero. We denote by $2c_0$ the total concentration of free ions in the bath, so that c_0 is the concentration of each ionic species. As the system evolves, the ECM increases in size until it reaches a steady state which is characterised by the continuity of chemical potentials and stresses across the boundary:

$$[\mu_s]_-^+ = [\mu_+]_-^+ = [\mu_-]_-^+ = 0, \quad [\mathbf{n}\mathbb{T}\mathbf{n}]_-^+ = 0. \tag{64}$$

As in [16], we consider that at equilibrium the following conditions also holds:

1. chemical potentials of solvent and solutes is homogeneous and equal in the bath and in the bath:

$$\mu_s = \mu_s^{ext} = \mu_s^0 - vkT \sum_i c_0^i, \tag{65}$$

$$\mu_i = \mu_i^{ext} = \mu_i^0 + kT \ln(v_s c_0^i). \tag{66}$$

2. The electrostatic potential and the solute concentration are constant in the ECM, but different to the value in the bath. This difference creates a thin charged interface at the boundary, whose thickness is negligible compared to the size of the ECM.
3. The contribution of $\mathbb{T}^{Max}$ and $\mathbb{T}^{kort}$to the stress at this interface can be neglected compared to the mechanical stress due to the deformation.
4. The Cauchy stress tensor is constant in the ECM and equal to the value in the bath:

$$\mathbb{T} = 0. \tag{67}$$

Finally, in order to characterise the equilibrium, we need to specify the deformation gradient tensor, which is of the form:

$$\mathbb{F} = \lambda \mathbb{I}, \tag{68}$$

with $\lambda = (1 + C_s v_s)^{1/3}$. Throughout the work, unless differently specified, we will use the parameters listed in Table 2 in Appendix (E).

As shown in Appendix F, imposing the equilibrium condition to both model A and B, we obtain that the nominal concentration of oxygen in the gel at equilibrium is implicitly defined by the algebraic equation:

$$\begin{aligned} F_A(C_s; c_0, \chi, G_{eq}^A) =& \frac{1 + C_s v_s + \chi}{(1 + C_s v_s)^2} + \frac{p v_s}{k_B T} + \ln \frac{C_s v_s}{1 + C_s v_s} + 2 c_0 v_s \\ & - \sqrt{\left(\frac{z_f C_f}{C_s}\right)^2 + 4 v_s^2 c_0^2} = 0 \end{aligned} \tag{69}$$

where the pressure p is defined according to the model used as:

$$p = \begin{cases} \frac{G^A_{eq}}{1+C_s v_s}(\lambda^2 - 1) & \text{MODEL A} \\ \frac{G^B_{vol}}{1+C_s v_s}(\lambda^2 - 1) & \text{MODEL B.} \end{cases} \tag{70}$$

where $G^A_e q = G^A_1 + G^A_2$. In this case, both model reduces to the standard hyperelastic model for polyelectrolytes proposed by Hong [23]. The most important characteristic of the model are summarised in Figure 8, which highlights the effect of different ion concentration in the bath on the degree of swelling. The behaviour is also sensitive to the value of the mixing parameter χ, which can be manipulated controlling the temperature. Depending on the latter, the ECM will either be in a highly swollen or collapsed phased with really low absorption of fluid [47].

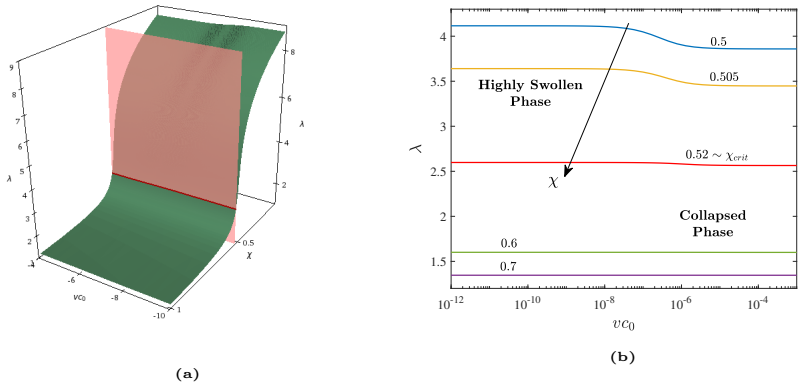

Fig. 8: Free Swelling: (a) Manifold implicitly defined by Equation (69) where $G^A_{eq} = 10^3$ is fixed, while c_0 and χ are varied. On the vertical axis, we have plot λ as defined by (68). In the red, it is highlighted the plane corresponding to $\chi = \chi_{crit}$ that split the parameter space into the region of high swelling and collapse for the material [].

As the model are equivalent, we conclude that common unconstrained swelling experiments that test the equilibrium state are not sufficient to discern between the two, but can be useful to estimate some of the several parameter in the model.

6 Confined Compression Test.

As a second experiment, we consider to perform compression test on a previously swollen slice of ECM. We assume to have estimated the value of χ, $G^A_{eq} \equiv G_{vol}$ based on the previously illustrated free swelling experiment. As illustrated in Figure 9, a porous platen is used so that the fluids is free to flow and the chemical equilibrium with the external bath is restored after the transient relaxation phase. After compression of the tissue in ramps, the system is allowed to relax while the strain ϵ is maintained constant [36]. In this case we are interested in the equilibrium, i.e. relaxed, behaviour.

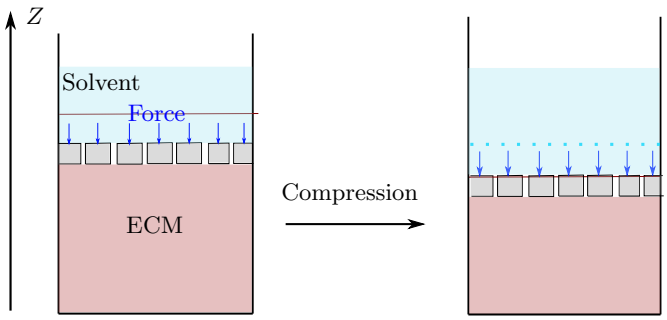

Fig. 9: Schematic representation of a compression test with a porous piston. A deformation is imposed in the Z direction and the force necessary to maintain the deformation is recorded.

As the deformation is constrained to the Z direction, the deformation tensor is of the form:

$$\mathbb{F} = J_0^{1/3} \begin{bmatrix} 1 & 0 & 0 \\ 0 & 1 & 0 \\ 0 & 0 & \lambda_1 \end{bmatrix}, \tag{71}$$

where $\lambda_1 = 1 - \epsilon$. The appropriate boundary condition in this case are:

$$[\mu_s]_-^+ = [\mu_+]_-^+ = [\mu_-]_-^+ = 0, \qquad Z = H_0 \quad [\mathbf{n}\mathbb{T}\mathbf{n}]_-^+ = 0, \qquad Z = 0, H_0, \mathbf{J}_s = \tag{72}$$

We here restrict our analysis to the equilibrium behaviour, for which the boundary conditions listed in Section 5.1 still hold with exception to the last one. Due to the external force $\mathbf{F} = -F_z \mathbf{e}_z$ which is exerted on the platen of area A, we now have that:

$$\mathbb{T} = \begin{bmatrix} 0 & 0 & 0 \\ 0 & 0 & 0 \\ 0 & 0 & \sigma \end{bmatrix}, \qquad \sigma = -\frac{F_z}{A}. \tag{73}$$

where $\mathbf{e}_z$ is the unit vector in the z direction in the current configuration. As we will see also in this simplified setting where the dynamics is neglected important differences emerges between the two model presented, which result in relevant quantitative predictions. Our aim is thus to understand under which information is necessary in order to discern which one better describe the material studied.

6.1 Model A

As before, given the symmetries of the system, $\mathbb{B}_e$ is a diagonal matrix of the form:

$$\mathbb{B}_e = \begin{bmatrix} b & 0 & 0 \\ 0 & b & 0 \\ 0 & 0 & b_1 \end{bmatrix}. \tag{74}$$

Again we are here interested in the equilibrium behaviour, for which Equations (**??**) still holds. Focusing on the contribution of spring B, studying the

equilibriums of Equation (54), we obtain that $b = b_1$. Since $\det \mathbb{B}_e = (\det \mathbb{F})^2$, we conclude that:

$$b = J_0^{2/3}\lambda_1^{2/3}. \tag{75}$$

Using the boundary condition, we can now compute the pressure and the equilibrium condition:

$$p = -\sigma + \frac{G_1^A}{J_0\lambda_1}(J_0^{2/3}\lambda_1^2 - 1) + \frac{G_2^A}{J_0\lambda_1}(J_0^{2/3}\lambda_1^{2/3} - 1) \tag{76}$$

$$\begin{aligned}\frac{\sigma v_s}{k_B T} =& \frac{J_0\lambda_1 + \chi}{J_0^2\lambda_1^2} + \frac{G_1^A v_s}{k_B T}\frac{J_0^{2/3}\lambda_1^2 - 1}{J_0\lambda_1} + \frac{G_2^A v_s}{k_B T}\frac{J_0^{2/3}\lambda_1^{2/3} - 1}{J_0\lambda_1} \\ &+ \ln\frac{J_0\lambda_1 - 1}{J_0\lambda_1} + 2c_0 v_s - \sqrt{\left(\frac{z_f C_f v_s}{J_0\lambda_1 - 1}\right)^2 + 4v_s^2 c_0^2}\end{aligned} \tag{77}$$

6.2 Models B.

Based on Equation (71), we have that the tensors $\bar{\mathbb{B}}$ and $\bar{\mathbb{B}}_e$ are of the form:

$$\bar{\mathbb{B}} = \begin{bmatrix} \lambda_1^{-2/3} & 0 & 0 \\ 0 & \lambda_1^{-2/3} & 0 \\ 0 & 0 & \lambda_1^{4/3} \end{bmatrix}, \qquad \bar{\mathbb{B}}_e = \begin{bmatrix} \bar{b} & 0 & 0 \\ 0 & \bar{b} & 0 \\ 0 & 0 & \bar{b}_1 \end{bmatrix} \tag{78}$$

As for the model A, at equilibrium we have that $\bar{b} = \bar{b}_1$. However, in this case, we have that $\det \bar{B}_e = 1$ so that $\bar{b} = 1$ so that the second spring does not contribute to the stress. Using the boundary condition, in the case of model BA we obtain:

$$p_B = -\sigma + \frac{G_{vol}}{J_0\lambda_1}(J_0^{2/3}\lambda_1^{2/3} - 1) + \frac{2G_1^B}{3J_0\lambda_1^{5/3}}(\lambda_1^2 - 1) \tag{79}$$

$$\begin{aligned}\frac{\sigma v_s}{k_B T} =& \frac{J_0\lambda_1 + \chi}{J_0^2\lambda_1^2} + \frac{2G_1^B v_s}{3k_B T}\frac{\lambda_1^2 - 1}{J_0\lambda_1^{5/3}} + \frac{G_{vol} v_s}{k_B T}\frac{J_0^{2/3}\lambda_1^{2/3} - 1}{J_0\lambda_1} \\ &+ \ln\frac{J_0\lambda_1 - 1}{J_0\lambda_1} + 2c_0 v_s - \sqrt{\left(\frac{z_f C_f v_s}{J_0\lambda_1 - 1}\right)^2 + 4v_s^2 c_0^2}.\end{aligned} \tag{80}$$

Unlike the case of unconstrained swelling, we now have that the model A and BA are substantially different, so that there is no choice of the parameter that would predict the same stress-strain behaviour. This highlights how, the choice of a particular decomposition of the deformation gradient $\mathbb{F}$ correspond to a modelling decision on the constitutive properties of the material under study.

6.3 Model Comparison.

We first focus on comparing the model A and AB, assuming that the parameter χ is fixed and that $G_{vol} = G_{eq}^A$, so that the equilibrium volume J_0 is the same

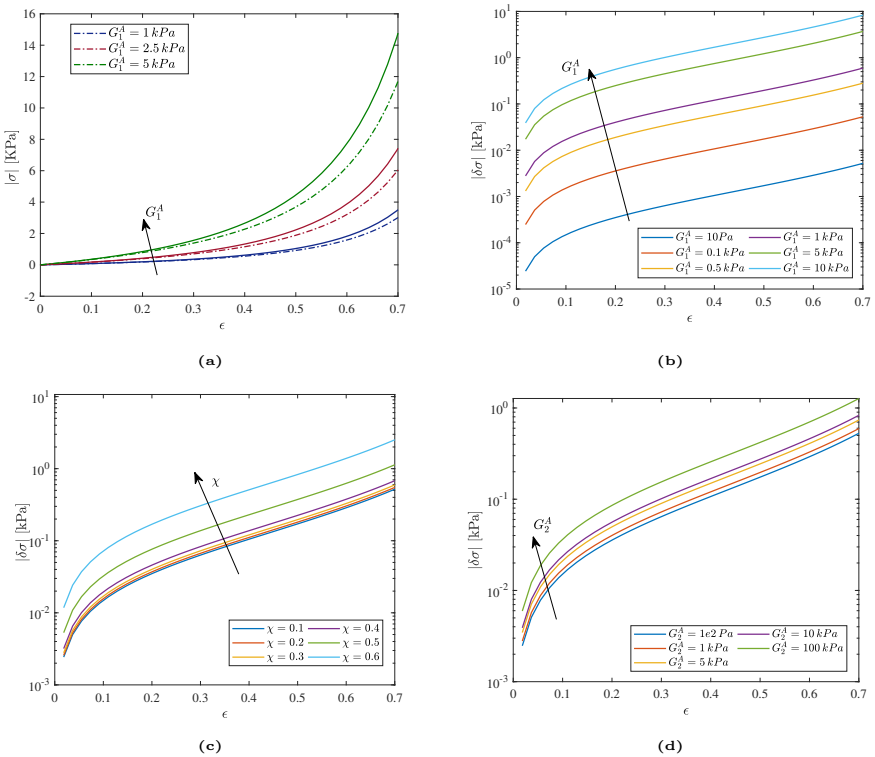

Fig. 10: Sensitivity Analysis. As expected the mismatch between the two model grows with the strain: (a) Comparison of stress-strain curve predicted by model A (dotted line) and model B (full line) for different value of the parameter G_1^A; (b) as G_1^A increase also the discrepancy $\delta\sigma$ grows; (c) $\delta\sigma$ is also particularly sensitive to changes in the mixing parameter χ, in particular we see that there is a relevant jump when the ECM is the *collapsed* phase; (d) on the other hand, only large changes in G_2^A have a relevant impact on $\delta\sigma$.

for both models. If we now take the difference between Equations (77) and (80), we obtain that the difference in the compression stress $\delta\sigma = \sigma_{BA} - \sigma_A$ is:

$$\delta\sigma = \frac{2G_1^B}{3}\frac{\lambda_1^2 - 1}{J_0\lambda_1^{5/3}} - \frac{G_1^A}{J_0^{1/3}}(\lambda_1 - \lambda_1^{-1/3}). \tag{81}$$

Looking at the above equation it appears clearly that there is no constant value of G_1^{AB} for which the difference $\delta\sigma$ is identically zero. If we impose that for small deformation, i.e. $\lambda_1 \to 1$, the two models agree at the second order:

$$\delta\sigma = 0, \qquad \frac{\mathrm{d}\delta\sigma}{\mathrm{d}\lambda_1} = 0 \quad \Rightarrow \quad G_1^B = J_0^{2/3}G_1^A. \tag{82}$$

Under such condition we can rewrite the Equation (81) as:

$$\delta\sigma(\lambda_1; G_1^A, J_0) = \frac{G_1^A}{J_0^{1/3}\lambda_1^{5/3}}\left(\frac{2}{3}\lambda_1^2 - \frac{2}{3} - \lambda_1^{5/3} + \lambda_1^{4/3}\right), \tag{83}$$

which is unbounded for large deformation, i.e. $\lambda_1 \Rightarrow 0$. Note that J_0 is implicitly defined by Equation (69), where $J_0 = 1 + v_s C_s$. Consequently $\delta\sigma$ depends also

on all the other parameters of the problem. As shown in Figure 10, χ plays an important role in determining the agreement between the two models. In our analysis, we have deliberately decided to look at absolute instead of relative differences. This is because when study the mechanical properties of materials, the order of magnitude are relevant in particular for scaffolds where pressure regulates the response of cells.

6.4 Test on Experimental Data.

In the previous section we have compared the two models assuming that data on free swelling are also available, so that G^A_{eq}, or equivalently G_{vol}, can be estimated separately, with all the other parameter known. However, this is not usually the case. In particular, when testing real tissues already swollen J_0 is not known and needs also to be estimated. Moreover, at our knowledge there are no studies on the estimation of the mixing parameter χ, so that this must be added to the list of unknown parameters.

Using the data collected by Netti et al. [36], we test the

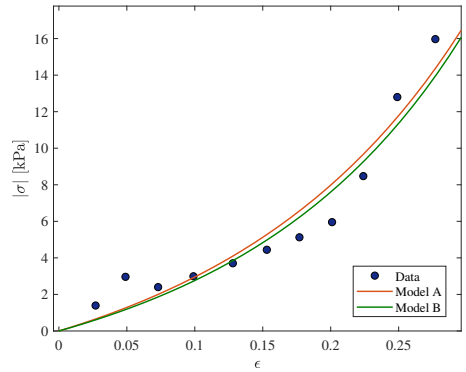

(a) Fitted Model

Model A		Model B	
χ	0.498	χ	0.524
G^A_1	18.9 kPa	G_{vol}	75 Pa
G^A_2	5.3 Pa	G^{BA}_1	55.1 kPa
J_0	20.7	J_0	14.8

(b) Estimated Parameters

Fig. 11: Comparison of the two model in fitting real experimental data from [36].

As shown in Figure 11a, both models are able to capture the qualitative behaviour of the data. However, as shown by the parameters in Table 11b, there are quantitative differences. In particular, there are order of magnitude of difference in the estimated pressure p. If we look at its value for zero-strain, i.e. $\lambda_1 = 1$, we obtain:

$$p_A = \frac{G^A_1 + G^A_2}{J_0}(J_0^{2/3} - 1) = \frac{24.2 \text{ kPa}}{20.7}(20.7^{2/3} - 1) = 7.64 \text{ kPa}, \tag{84}$$

$$p_{BA} = \frac{G_{vol}}{J_0}(J_0^{2/3} - 1) = \frac{0.075 \text{ kPa}}{14.8}(14.8^{2/3} - 1) = 25.5 \text{ Pa} \tag{85}$$

When designing synthetic ECM, the tuning of the internal pressure cells in a culture are exposed to is of large importance. As mentioned in the introduction, cells are sensitive to pressure and their response can greatly change depending on this stimulus. Consequently, depending on the model chosen, the

A Glossary of Variables and Parameters in the Model.

ψ	Helmholtz free energy per unit volume in the initial configuration,
$\mathbf{u}$	Displacement vector,
$\mathbb{F}$	Deformation gradient tensor $\mathbb{F} = \mathbb{I} - \nabla_0 \mathbf{u}$,
C_f	Concentration of fix charges in the network,
z_f	Charge of a GAG chain,
v_m	Characteristic molecular volume of the species m,
$\mathbf{u}$	Displacement vector,
$\mathbb{F}$	Deformation gradient tensor $\mathbb{F} = \mathbb{I} - \nabla_0 \mathbf{u}$,
$\mathbb{C}$	Right Cauchy-Green Tensor $\mathbb{C} = \mathbb{F}^T\mathbb{F}$,
$\mathbb{B}$	Left Cauchy-Green Tensor $\mathbb{B} = \mathbb{F}\mathbb{F}^T$,
$\mathbb{L}$	Velocity Gradient Tensor $\mathbb{L} = \dot{\mathbb{F}}\mathbb{F}^{-1}$,
J	Determinant of the deformation gradient tensor $J = \det \mathbb{F}$,
η^A	Viscosity of the collagen network in model A,
G_1^A	Shear modulus related to spring 1 in model A
G_2^A	Shear modulus related to spring 2 in model A
G_1^B	Shear modulus related to spring 1 in model B
G_2^B	Shear modulus related to spring 2 in model B
η^B	Viscosity of the collagen network in model A,
τ_R	Viscous relaxation time of the collagen network,
D_i^0	Diffusion coefficient for the i-th solute species when in pure solvent (interstitial fluid),
D_i	Diffusion coefficient for the i-th solute species in ECM,
K	Hydraulic permeability of the ECM to the interstitial fluid (solvent+solute),
k	Hydraulic permeability to pure solvent (water),
κ	Bulk modulus
$\mathbb{T}^{Kort}$	Korteweg stress due to the ideal interface
$\mathbb{T}^{Max}$	Maxwell stress due to the electric displacement
k_B	Boltzmann constant
T	Absolute Temperature
$\mathrm{DEV}\,[\cdot]$	Deviatoric part of the tensor $\mathrm{DEV}\,[\cdot] = \cdot - 1/3\,\mathrm{tr}(\cdot)$

B

$$\boldsymbol{\xi} = \frac{\partial \psi}{\partial \nabla_0 C} =, \tag{86}$$

$$\mu = \frac{\partial \psi}{\partial C} - \nabla_0 \cdot \boldsymbol{\xi} + pv, \tag{87}$$

$$\mathbb{S} = \frac{\partial \psi}{\partial \mathbb{F}} + \frac{\partial \psi}{\partial \mathbb{F}_e}\mathbb{F}_v^{-T} - pJ\mathbb{F}^{-T} \tag{88}$$

C Energy Dissipation.

Combining Equation (48) and (50), and imposing that condition (23) is satisfied, we can characterise the viscous flow by the following relation:

$$\mathbb{L}_v = L_{vv} T^{-1} \left[\mathbb{F}_e^T \frac{\partial \psi}{\partial \mathbb{F}_e} - p_v \mathbb{I} \right] \overset{(*)}{=} \frac{G_2^A}{\eta^A} \mathrm{DEV}\left[\mathbb{C}_e\right], \tag{89}$$

where η^A represent the viscosity of the material and the equality $(*)$ follows from Equation (32):

$$\eta^A tr(\mathbb{L}_v) = tr\left(\mathbb{F}_e^T \frac{\partial \psi}{\partial \mathbb{F}_e} \right) - 3p_v = 0 \Longrightarrow p_v = \frac{tr\left(\mathbb{F}_e^T \frac{\partial \psi}{\partial \mathbb{F}_e} \right)}{3}. \tag{90}$$

Using Equation (41), we obtain:

$$\mathbb{L}_v = \frac{G_2^A}{\eta^A} \mathrm{DEV}[\mathbb{C}_e] = \frac{\mathrm{DEV}[\mathbb{C}_e]}{2\tau_R}. \tag{91}$$

If we now consider the left elastic Cauchy Green tensor $\mathbb{B}_e = \mathbb{F}_e \mathbb{F}_e^T$, we can relate its time derivative to $\mathbb{L}_v$:

$$\begin{aligned} \dot{\mathbb{B}}_e &= \mathbb{L}\mathbb{B}_e + \mathbb{B}_e \mathbb{L}^T - 2\mathbb{F}_e d_v \mathbb{F}_e^T \\ &= \mathbb{L}\mathbb{B}_e + \mathbb{B}_e \mathbb{L}^T - \frac{1}{\tau_R} \mathbb{F}_e \left[\mathbb{C}_e - \frac{1}{3} tr(\mathbb{B}_e) \mathbb{I} \right] \mathbb{F}_e^T \\ &= \mathbb{L}\mathbb{B}_e + \mathbb{B}_e \mathbb{L}^T - \frac{1}{\tau_R} \mathbb{B}_e \underbrace{\left[\mathbb{B}_e - \frac{1}{3} tr(\mathbb{B}_e) \mathbb{I} \right]}_{\mathrm{DEV}[\mathbb{B}_e]}. \end{aligned} \tag{92}$$

For what concern the dissipation due to transport phenomena, the forces ς_m is dependent on the deformation. For this reason, it is more suitable to move from the Lagrangian to the Eulerian coordinates. Using the can rewrite the flux as $\mathbf{j}_m = c_m(\mathbf{v}_m - \mathbf{v}_n) = c_m \bar{\mathbf{v}}_m$, where $\mathbf{v}_m$ is the velocity of the m-th component in the current configuration, $\mathbf{v}_n$ is the velocity of the network also in the current configuration and $\bar{\mathbf{v}}_m$ is the relative velocity of the m-th component with respect to the network.

In the framework of linear non-equilibrium thermodynamics, the transport dissipation function is given by:

$$-c_j \nabla \mu_j = \sum_b L_{jb} \bar{\mathbf{v}}_j = \sum_{i \neq j} f_{ji} \left(\bar{\mathbf{v}}_i - \bar{\mathbf{v}}_j \right) + f_{js} (\bar{\mathbf{v}}_s - \bar{\mathbf{v}}_j) + f_{jn} \bar{\mathbf{v}}_j, \tag{93}$$

$$-c_s \nabla \mu_s = \sum_i f_{si} \left(\bar{\mathbf{v}}_i - \bar{\mathbf{v}}_s \right) + f_{sn} \bar{\mathbf{v}}_s, \tag{94}$$

where f_{mi} and h_{mn} are the drag coefficients related to the interaction between fluid constituents and the polymer network respectively. Based on the Onsanger's reciprocal relation we have that:

$$f_{mb} = f_{bm}. \tag{95}$$

Common assumption in the study of mixture theory is that the solute-solute drag can be neglected so that $f_{ij} = 0$ for $i, j = 1, \dots, N$ [44,**?**]. The remaining drag coefficient are instead defined by:

$$f_{sn} = \frac{1}{k}, \quad f_{js} = \frac{k_B T c_j}{D_j^0}, \quad f_{js} + f_{jn} = \frac{k_B T c_j}{D_j}, \tag{96}$$

where k is the hydraulic permeability of the solvent in the network, D_j^0 is the diffusion coefficient of the solute in pure solution, while D_j is the diffusion coefficient in the gel.

Using (93)-(96), the relative velocities are of the form:

$$\bar{\mathbf{v}}_s = -KJ\left(\nabla\mu_s + \sum_i \frac{D_i}{D_i^0}\frac{C_i}{C_s}\nabla\mu_i\right), \tag{97}$$

$$\bar{\mathbf{v}}_j = -\frac{D_j}{k_B T}\nabla\mu_j + \frac{D_j}{D_j^0}\bar{\mathbf{v}}_s, \tag{98}$$

and the coefficient K is defined as:

$$\frac{1}{K} = \frac{J}{c_s k} + \sum_i \frac{k_B T}{\phi_w}\left(1 - \frac{D_i}{D_i^0}\right)\frac{C_i}{D_i^0}. \tag{99}$$

D Model B: Separating the Volumetric Deformation.

The derivation of the governing equation for the second model proposed follow the same steps as model A, with few changes. From the point of view of conservation laws (Section 4.1), these are still valid as they do not depend on the specific kinetics model chosen. As discussed in Section 4.2, we use multiplicative decomposition to isolate the different contribution to the strain:

$$\mathbb{F} = \bar{\mathbb{F}}\mathbb{F}_{vol} = J^{1/3}\bar{\mathbb{F}}_e\bar{\mathbb{F}}_v, \tag{100}$$

where we have used the fact that $\mathbb{F}_{vol} = J^{1/3}\mathbb{I}$, with $J = \det\mathbb{F}$. Where both $\bar{\mathbb{F}}_e$ and $\bar{\mathbb{F}}_v$ needs to preserve the ECM volume. Analogously to Equation (23), this can be ensured by imposing the following condition:

$$\det\bar{\mathbb{F}}_v = 1. \tag{101}$$

In this case it is easier to express the kinematics of the ECM in terms $\mathbb{L} = \dot{\mathbb{F}}\mathbb{F}^{-1}$, instead of $\dot{\mathbb{F}}$ and $\bar{\mathbb{L}}_v = \dot{\bar{\mathbb{F}}}_v\bar{\mathbb{F}}_v^{-1}$. When we look at the free energy, we now have three decouple mechanical variables that can contribute to it J for the first spring, $\bar{\mathbb{F}}$ and $\bar{\mathbb{F}}_e$ on due to the springs in branch **A** and **B** respectively. Consequently, Equation (30) will now be of the form:

$$\psi = \psi(J, \bar{\mathbb{F}}_e, \bar{\mathbb{F}}, C_s, C_i, \nabla_0 C_s, \mathbf{H}). \tag{102}$$

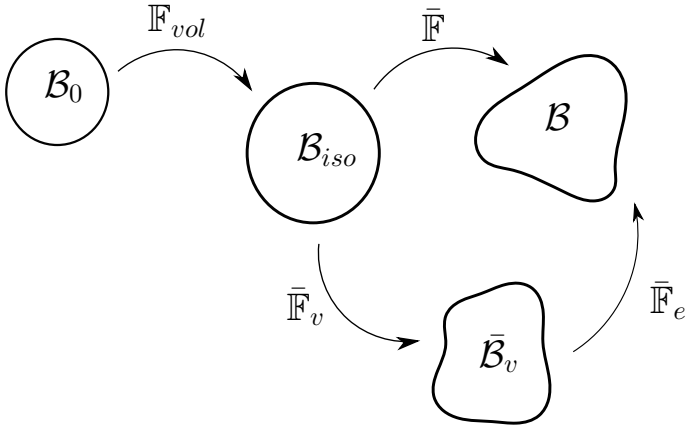

Fig. 12: Multiplicative decomposition of Model B

If we differentiate J, $\bar{\mathbb{F}}$ and $\bar{\mathbb{F}}_e$, we can reduce the number of variables expressing them in terms of $\mathbb{L}$ and $\bar{\mathbb{L}}_v$:

$$\dot{J} = J(\mathbb{I} : \mathbb{L}), \tag{103}$$

$$\dot{\bar{\mathbb{F}}} = J^{-1/3}\mathbb{L}\mathbb{F} - \frac{1}{3}J^{-1/3}(\mathbb{I} : \mathbb{L})\mathbb{F} \tag{104}$$

$$\dot{\bar{\mathbb{F}}}_e = \mathrm{DEV}[\mathbb{L}]\bar{\mathbb{F}}_e - \bar{\mathbb{F}}_e\bar{\mathbb{L}}_v. \tag{105}$$

If we now combine Equations (102)-(105) with the energy inequality, what we obtain is:

$$\begin{aligned}
&\left(\frac{\partial\psi}{\partial\nabla_0 C_s} - \boldsymbol{\xi}\right)\cdot\nabla_0\dot{C}_s + \left(\frac{\partial\psi}{\partial C_s} - \mu_s - \nabla_0\cdot\boldsymbol{\xi} + pv\right)\dot{C}_s \\
&\qquad + \sum_i\left(\frac{\partial\psi}{\partial C_i} + e\Phi z_i - \mu_i\right)\dot{C}_i + \left(\frac{\partial\psi}{\partial\mathbf{H}} - \mathbf{E}\right)\cdot\dot{\mathbf{H}} \\
&+ \left(\mathrm{DEV}\left[J^{-1/3}\frac{\partial\psi}{\partial\bar{\mathbb{F}}}\mathbb{F}^T + \frac{\partial\psi}{\partial\bar{\mathbb{F}}_e}\bar{\mathbb{F}}_e^T\right] - \mathbb{S}\mathbb{F}^T + J\left(\frac{\partial\psi}{\partial J} - p\right)\mathbb{I}\right) : \mathbb{L} \\
&\qquad + \sum_m \nabla_0\,\mu_m\cdot\mathbf{J}_m - \bar{\mathbb{F}}_e^T\frac{\partial\psi}{\partial\bar{\mathbb{F}}_e} : \bar{\mathbb{L}}_v \le 0.
\end{aligned} \tag{106}$$

Finally we need to update the constitutive laws for the strain free energy ψ_6, which, similarly to the case discussed in Section , can be decompose as the sum of contributions from each spring in Figure **??**(b):

$$\psi_6 = \psi_1(\bar{\mathbb{F}}) + \psi_2(\bar{\mathbb{F}}_e) + \psi_{vol}(J). \tag{107}$$

Again we assume the ECM to behave as an hyperplastic material:

$$\psi_1(\bar{\mathbb{F}}) = \frac{G_1^B}{2}\left(\bar{\mathbb{F}} : \bar{\mathbb{F}} - 3\right), \tag{108}$$

$$\psi_2(\bar{\mathbb{F}}_e) = \frac{G_2^B}{2}\left(\bar{\mathbb{F}}_e : \bar{\mathbb{F}}_e - 3\right). \tag{109}$$

For the volumetric contribution we consider as before a logarithmic term:

$$\psi_{vol}(J) = \frac{\kappa}{2}\ln J^2. \tag{110}$$

ALTERNATIVE:

$$\psi_{vol}(J) = \frac{G_{vol}}{2}\left[3(J^{2/3} - 1) - \ln J^2\right]. \tag{111}$$

The above volumetric constitutive assumption is one of the most common in modelling hyper-elastic material. However, as shown in [35], this has several limitation in the regime of large deformation, which highlights the need of study more realistic form which can capture the more complex behaviour of real material. From this point of view, being able to decouple the volumetric deformation as in model B allows to investigate this aspect alone [REPHRASE].

When looking at the entropy production, Equation (42) still holds simply by replacing $\mathbb{L}_v$ with $\bar{\mathbb{L}}_v$:

$$\mathbb{L}_v = \frac{G_2^B}{\eta^B}\mathrm{DEV}[\bar{\mathbb{C}}_e] \tag{112}$$

Using the same argument as in Section (4.5), we are left with the following system of equations:

$$\boldsymbol{\xi} = \gamma J\, \mathbb{B}^{-1}\, \nabla_0\, C_s, \tag{113}$$

$$\begin{aligned}\mu_s = pv + \mu_s^0 - \gamma J \nabla^2 C_s + kT\Bigg[&\ln\frac{C_s v}{1 + C_s v} + \frac{1}{1 + C_s v} \\ &+ \frac{\chi}{(1 + C_s v)^2} - \sum_i \frac{C_i}{C_s}\Bigg],\end{aligned} \tag{114}$$

$$\mu_i = \mu_i^0 + e\Phi z_i + kT\ln\frac{C_i}{C_s}, \tag{115}$$

$$\mathbf{E} = \frac{1}{\epsilon J}\mathbb{F}^T\mathbb{F}\,\mathbf{H} \tag{116}$$

$$\begin{aligned}\mathbb{T} = &\left(\frac{\kappa}{1 + C_s v_s} - p\right)\mathbb{I} + \frac{G_1^B}{1 + C_s v}\mathrm{DEV}[\bar{\mathbb{B}}] + \frac{G_2^B}{1 + C_s v}\mathrm{DEV}[\bar{\mathbb{B}}_e] \\ &+\gamma\left[\frac{1}{2}|\nabla C_s|^2\mathbb{I} - \nabla C_s \otimes \nabla C_s\right] + \epsilon\left[\frac{1}{2}\,|\nabla\Phi|^2\mathbb{I} - \nabla\Phi \otimes \nabla\Phi\right],\end{aligned} \tag{117}$$

coupled to the governing equations:

$$\mathbf{j}_s = -Kc_s\left(c_s\nabla\mu_s + \sum_i \frac{D_i}{D_i^0}c_i\nabla\mu_i\right), \tag{118}$$

$$\mathbf{j}_i = -\frac{D_i}{k_BT}c_i\nabla\mu_i + \frac{D_i}{D_i^0}\frac{c_i}{c_s}\mathbf{j}_s, \tag{119}$$

$$\dot{\bar{\mathbb{B}}}_e = \bar{\mathbb{B}}_e\bar{\mathbb{L}}^T + \bar{\mathbb{L}}\bar{\mathbb{B}}_e - \frac{1}{\tau_R}\bar{\mathbb{B}}_e\mathrm{DEV}\left[\bar{\mathbb{B}}_e\right] \tag{120}$$

E Simulation Parameter.

Throughout the work, unless differently specified, we will use the parameters in Table 2 will be considered to be constant so to reflect the condition in the experiment by Netti et al. [36,45].

Symbol	Value	Unit
C_f	3.947×10^{23}	m^{-3}
v_s	3×10^{-29}	m^3
z_f	-4	-
k_B	1.38×10^{-23}	J/K
T	295	K
c_0^i	9.27×10^{25}	m^{-3}

Table 2: Parameters adopted in the simulations as estimated in [45] in reference to the experiment by Netti et al. [36].

F Free Swelling

In the case of free swelling, due to the symmetry of $\mathbb{F}$, the tensors $\mathbb{F}_e$ and $\bar{F}_e$ is of the similar form, $\mathbb{F}_e = \lambda_e\mathbb{I}$. Consequently, based on Equation (91) in Appendix C, we have that the viscous contribution vanish so that $\mathbb{B}_e = \mathbb{B} = \lambda^2\mathbb{I}$. Substituting this result and the boundary condition (66)-(67) into Equations (**??**)-(45) and

(46), setting to zero all spatial derivative, we obtain:

$$p_A = \frac{G_1^A + G_2^A}{1 + C_s v_s}(\lambda^2 - 1), \tag{121}$$

$$\Pi_A^n = \frac{k_B T}{v_s}\left[\ln\frac{C_s v_s}{1 + C_s v_s} + \frac{1}{1 + C_s v_s} + \frac{\chi}{(1 + C_s v_s)^2}\right], \tag{122}$$

$$\Pi_A^{ion} = k_B T \sum_i \left(\frac{C_i}{v_s C_s} - c^0\right), \tag{123}$$

$$0 = \frac{v_s}{k_B T}(p_A + \Pi_A^n - \Pi_A^{ion}), \tag{124}$$

$$0 = \pm\frac{e}{k_B T}\phi + \ln\frac{C_\pm}{C_s v_s c_\pm^0}, \qquad i = 1, \ldots, N, \tag{125}$$

$$Q = e\,(C_+ - C_- + z_f C_f) = 0. \tag{126}$$

where Π^n and Π_A^{ion} are the osmotic pressures due to the mixing of the polymer network with the solvent and the imbalance of ions inside and outside the ECM. Note that at equilibrium the system reaches a balance between the mechanical pressure p_A and the osmotic pressures. Moreover, the electro-neutrality condition is naturally imposed, Equation (126). Note that Equation (**??**) corresponds to the well known Donnan Equilibrium [16]. Equation (69) instead implicitly defines the concentration C_s and thus the final swelling volume. As expected, the latter can be controlled by changing the concentration of ions in the bath. We also notice that, free swelling experiment, are not sufficient to differentiate the elastic properties of the two branches as the two behave equivalently.

References

1. Anand, L.: A thermo-mechanically-coupled theory accounting for hydrogen diffusion and large elastic–viscoplastic deformations of metals. International Journal of Solids and Structures **48**(6), 962 – 971 (2011)
2. Benfenati, F., Beretta, G.P.: Ergodicity, Maximum Entropy Production, and Steepest Entropy Ascent in the Proofs of Onsager's Reciprocal Relations. Journal of Non Equilibrium Thermodynamics **43**, 101–110 (Apr 2018)
3. Beretta, G.P.: The fourth law of thermodynamics: steepest entropy ascent. arXiv preprint arXiv:1908.05768 (2019)
4. Bergström, J., Boyce, M.: Constitutive modeling of the large strain time-dependent behavior of elastomers. Journal of the Mechanics and Physics of Solids **46**(5), 931 – 954 (1998)
5. Bertet, C., Sulak, L., Lecuit, T.: Myosin-dependent junction remodelling controls planar cell intercalation and axis elongation. Nature **429**, 667–71 (07 2004)
6. Boyce, M.C., Arruda, E.M.: Constitutive models of rubber elasticity: A review. Rubber Chemistry and Technology **73**(3), 504–523 (2000)
7. Buenger, D., Topuz, F., Groll, J.: Hydrogels in sensing applications. Progress in Polymer Science **37**(12), 1678 – 1719 (2012)
8. Butcher, D., Alliston, T., Weaver, V.: A tense situation: forcing tumour progression. nat rev cancer 9: 108-122. Nature reviews. Cancer **9**, 108–22 (03 2009)
9. Caccavo, D., Cascone, S., Lamberti, G., Barba, A.A.: Hydrogels: experimental characterization and mathematical modelling of their mechanical and diffusive behaviour. Chem. Soc. Rev. **47**, 2357–2373 (2018)
10. Caccavo, D., Vietri, A., Lamberti, G., Barba, A.A., Larsson, A.: Modeling the mechanics and the transport phenomena in hydrogels. In: Manca, D. (ed.) Quantitative Systems Pharmacology, Computer Aided Chemical Engineering, vol. 42, chap. 12, pp. 357 – 383. Elsevier (2018)
11. Chaudhuri, O.: Viscoelastic hydrogels for 3d cell culture. Biomater. Sci. **5**, 1480–1490 (2017)
12. Cohen Stuart, M., Huck, W., Genzer, J., Müller, M., Ober, C., Stamm, M., Sukhorukov, G., Szleifer, I., Tsukruk, V., Urban, M., Winnik, F., Zauscher, S., Luzinov, I., Minko, S.: Emerging applications of stimuli-responsive polymer materials. Nature materials **9**, 101–13 (2010)
13. Deligkaris, K., Tadele, T.S., Olthuis, W., Van den Berg, A.: Hydrogel-based devices for biomedical applications. Sensors and Actuators B: Chemical **147**, 765–774 (2010)
14. Doi, M.: Soft Matter Physics. OUP Oxford (2013)
15. Drozdov, A.: Swelling of ph-responsive cationic gels: Constitutive modeling and structure–property relations. International Journal of Solids and Structures **64-65**, 176 – 190 (2015)
16. Drozdov, A.D., deClaville Christiansen, J., Sanporean, C.G.: Inhomogeneous swelling of ph-responsive gels. International Journal of Solids and Structures **87**, 11 – 25 (2016)
17. Flory, P.J.: Thermodynamics of high polymer solutions. The Journal of Chemical Physics **10**(1), 51–61 (1942)
18. Flory, P.: Principles of Polymer Chemistry. Baker lectures 1948, Cornell University Press (1953)
19. Garcia-Gonzalez, D., Jerusalem, A.: Energy based mechano-electrophysiological model of cns damage at the tissue scale. Journal of the Mechanics and Physics of Solids **125**, 22 – 37 (2019)

20. Garcia-Gonzalez, D.: Magneto-visco-hyperelasticity for hard-magnetic soft materials: theory and numerical applications. Smart Materials and Structures **28**(8), 085020 (jul 2019)
21. Gurtin, M.E.: Generalized ginzburg-landau and cahn-hilliard equations based on a microforce balance. Physica D: Nonlinear Phenomena **92**(3), 178 – 192 (1996)
22. Hennessy, M.G., Münch, A., Wagner, B.: Surface induced phase separation of a swelling hydrogel (2018), preprint on webpage `http://www.wias-berlin.de/preprint/2562/wias_preprints_2562.pdf`
23. Hong, W.: Continuum Models of Stimuli-responsive Gels, pp. 165–196. Springer Berlin Heidelberg, Berlin, Heidelberg (2012)
24. Hong, W., Wang, X.: A phase-field model for systems with coupled large deformation and mass transport. Journal of the Mechanics and Physics of Solids **61**(6), 1281 – 1294 (2013)
25. Hu, Y., Suo, Z.: Viscoelasticity and poroelasticity in elastomeric gels. Acta Mechanica Solida Sinica **25**(5), 441 – 458 (2012)
26. Huggins, M.L.: Some properties of solutions of long-chain compounds. The Journal of Physical Chemistry **46**(1), 151–158 (1942)
27. Kondepudi, D., Prigogine, I.: Modern Thermodynamics: From Heat Engines to Dissipative Structures. CourseSmart, John Wiley & Sons (2014)
28. Kröner, E.: Allgemeine Kontinuumstheorie der Versetzungen und Eigenspannungen. Archive for Rational Mechanics and Analysis **4**, 273–334 (1959)
29. Larché, F., Cahn, J.: The interactions of composition and stress in crystalline solids. Acta Metallurgica **33**(3), 331 – 357 (1985)
30. Lebon, G., Jou, D., José, C.V.: Understanding Non-Equilibrium Thermodynamics. Springer-Verlag Berlin Heidelberg (01 2008)
31. Levental, I., Georges, P.C., Janmey, P.A.: Soft biological materials and their impact on cell function. Soft Matter **3**, 299–306 (2007)
32. Li, J., Mooney, D.: Designing hydrogels for controlled drug delivery. Nature Reviews Materials **1**, 16071 (2016)
33. Lubarda, V.A.: Constitutive theories based on the multiplicative decomposition of deformation gradient: Thermoelasticity, elastoplasticity, and biomechanics . Applied Mechanics Reviews **57**(2), 95–108 (04 2004)
34. Marsland, R., England, J.: Limits of predictions in thermodynamic systems: a review. Reports on Progress in Physics **81**(1) (2017)
35. Moerman, K.M., Fereidoonnezhad, B., McGarry, P.: Novel hyperelastic models for large volumetric deformations (Feb 2019)
36. Netti, P.A., Berk, D.A., Swartz, M.A., Grodzinsky, A.J., Jain, R.K.: Role of extracellular matrix assembly in interstitial transport in solid tumors. Cancer Research **60**(9), 2497–2503 (2000)
37. N'Guyen, T., Lejeunes, S., Eyheramendy, D., Boukamel, A.: A thermodynamical framework for the thermo-chemo-mechanical couplings in soft materials at finite strain. Mechanics of Materials **95**, 158 – 171 (2016)
38. Onsager, L.: Reciprocal relations in irreversible processes. i. Phys. Rev. **37**, 405–426 (Feb 1931)
39. Paszek, M.J., Zahir, N., Johnson, K.R., Lakins, J.N., Rozenberg, G.I., Gefen, A., Reinhart-King, C.A., Margulies, S.S., Dembo, M., Boettiger, D., Hammer, D.A., Weaver, V.M.: Tensional homeostasis and the malignant phenotype. Cancer Cell **8**(3), 241 – 254 (2005)
40. Prigogine, I.: Introduction to thermodynamics of irreversible processes. Interscience Publishers (1968)

41. Rauzi, M., Vérant, P., Lecuit, T., Lenne, P.F.: Nature and anisotropy of cortical forces orienting drosophila tissue morphogenesis. Nature Cell Biology **10**, 1401–1410 (2008)
42. Sun, D.N., Gu, W.Y., Guo, X.E., Lai, W.M., Mow, V.C.: A mixed finite element formulation of triphasic mechano-electrochemical theory for charged, hydrated biological soft tissues. International Journal for Numerical Methods in Engineering **45**(10), 1375–1402 (1999)
43. Xue, S.L., Li, B., Feng, X.Q., Gao, H.: Biochemomechanical poroelastic theory of avascular tumor growth. Journal of the Mechanics and Physics of Solids **94**, 409 – 432 (2016)
44. Xue, S.L., Li, B., Feng, X.Q., Gao, H.: A non-equilibrium thermodynamic model for tumor extracellular matrix with enzymatic degradation. Journal of the Mechanics and Physics of Solids **104**, 32 – 56 (2017)
45. Xue, S.L., Lin, S.Z., Li, B., Feng, X.Q.: A nonlinear poroelastic theory of solid tumors with glycosaminoglycan swelling. Journal of Theoretical Biology **433**, 49 – 56 (2017)
46. Yu, Y., Landis, C.M., Huang, R.: Salt-Induced Swelling and Volume Phase Transition of Polyelectrolyte Gels. Journal of Applied Mechanics **84**(5) (03 2017)
47. Yu, Y., Landis, C.M., Huang, R.: Salt-Induced Swelling and Volume Phase Transition of Polyelectrolyte Gels. Journal of Applied Mechanics **84**(5) (03 2017). https://doi.org/10.1115/1.4036113, 051005